The Kelvin-Helmholtz Instability at CME-Boundaries in the Solar Corona: Observations and 2.5D MHD Simulations

U.V. Möstl, M. Temmer, and A.M. Veronig

IGAM-Kanzelhöhe Observatory, Institute of Physics, University of Graz, 8010 Graz, Austria

ute.moestl@uni-graz.at

Received _____; accepted _____

ABSTRACT

The Atmospheric Imaging Assembly onboard the Solar Dynamics Observatory observed a coronal mass ejection with an embedded filament on 2011 February 24, reavealing quasi-periodic vortex-like structures at the northern side of the filament boundary with a wavelength of approximately 14.4 Mm and a propagation speed of about 310 ± 20 km s^{-1}. These structures could result from the Kelvin-Helmholtz instability occurring on the boundary. We perform 2.5D numerical simulations of the Kelvin-Helmholtz instability and compare the simulated characteristic properties of the instability with the observations, where we obtain qualitative as well as quantitative accordance. We study the absence of Kelvin-Helmholtz vortex-like structures on the southern side of the filament boundary and find that a magnetic field component parallel to the boundary with a strength of about 20% of the total magnetic field has stabilizing effects resulting in an asymmetric development of the instability.

Subject headings: Instabilities — Magnetohydrodynamics (MHD) — Methods: numerical — Sun: corona — Sun: coronal mass ejections (CMEs)

1. Introduction

For the dynamics of the solar atmosphere, magnetohydrodynamic (MHD) instabilities are thought to play a major role (e.g. Ryutova et al. 2010; Foullon et al. 2011; Ofman & Thompson 2011; Taroyan 2011; Innes et al. 2012). Specifically, there are boundary layers, where the Kelvin-Helmholtz instability (KHI) might be able to develop, as treated in several theoretical studies on this topic (e.g. Heyvaerts & Priest 1983; Rae 1983; Karpen et al. 1993; Andries and Goossens 2001; Kolesnikov et al. 2004; Soler et al. 2010; Zaqarashvili et al. 2010; Soler et al. 2012). In principal, the KHI arises at boundaries with a velocity shear parallel to a boundary layer (Chandrasekhar 1961), and there exist many plasma configurations in space where the KHI can occur (e.g. Miura 1997, and references therein).

With the unprecedented observations by the Atmospheric Imaging Assembly (AIA; Lemen et al. 2012) onboard Solar Dynamics Observatory (SDO; Pesnell et al. 2012) it is possible to gain observational evidence for instabilities in the solar atmosphere. SDO/AIA carries four telescopes providing narrow-band full-disk imaging of the Sun in different UV and EUV passbands at a cadence as high as 12 s and spatial resolution of $1''.5$ (Lemen et al. 2012). Foullon et al. (2011) and Ofman & Thompson (2011) were the first to present observations of the KHI associated with a coronal mass ejection (CME). Ofman & Thompson (2011) analyzed a series of vortices seen along the boundary of an evolving coronal dimming region on 2010 April 8. They compared for the first time the observational features with the results of a 2.5D MHD model of the KHI and found good qualitative agreement. Foullon et al. (2011) reported observations of wavy vortex-like structures on one flank of a CME that occurred on 2010 November 3. These studies hint at the existence of the KHI in the solar corona. Yet, we need to have more observations and theoretical (numerical) studies on this subject to be clearly able to distinguish between

structures produced by the KHI and such that have a different origin.

In this letter, we report quasi-periodic vortex-like structures observed on the boundary of an erupting filament/CME on 2011 February 24 in SDO/AIA high cadence imagery. We follow a similar approach as Ofman & Thompson (2011) and give a detailed comparison of these observations and a 2.5D MHD simulation of the KHI. Qualitative as well as quantitative analyses of both spatial and temporal features are presented. Furthermore, we investigate the effect of a magnetic field component parallel to the boundary layer on the evolution of the instability and determine a threshold for the field strength needed to stabilize the boundary.

2. Observations and Analyses

On 2011 February 24, a CME eruption with an embedded filament was observed by the AIA instrument onboard SDO in association with a GOES M3.5 limb flare (Battaglia and Kontar 2011; Martínez Oliveros et al. 2012). The top three panels of Figure 1 show direct images in the AIA 304 Å passband (dominated by emission from He II; $\log(T) = 4.7$), the bottom panels display running difference images in the 171 Å channel (dominated by emission from Fe IX; $\log(T) = 5.8$; Lemen et al. 2012). On the right panel we show the associated CME observed by the Large Angle and Spectrometric Coronagraph (LASCO) C2 onboard the Solar and Heliospheric Observatory (SOHO). The insert (yellow rectangle) represents the AIA 171 Å running difference image recorded about 30 minutes before the LASCO image shown. The CME structure breaks up rather early in its evolution (around 07:30:00 UT), and quasi-periodic vortex-like structures develop around 07:36:00 UT on the northern side of the boundary of the filament embedded in the CME (see accompanying movie in the online version of this publication).

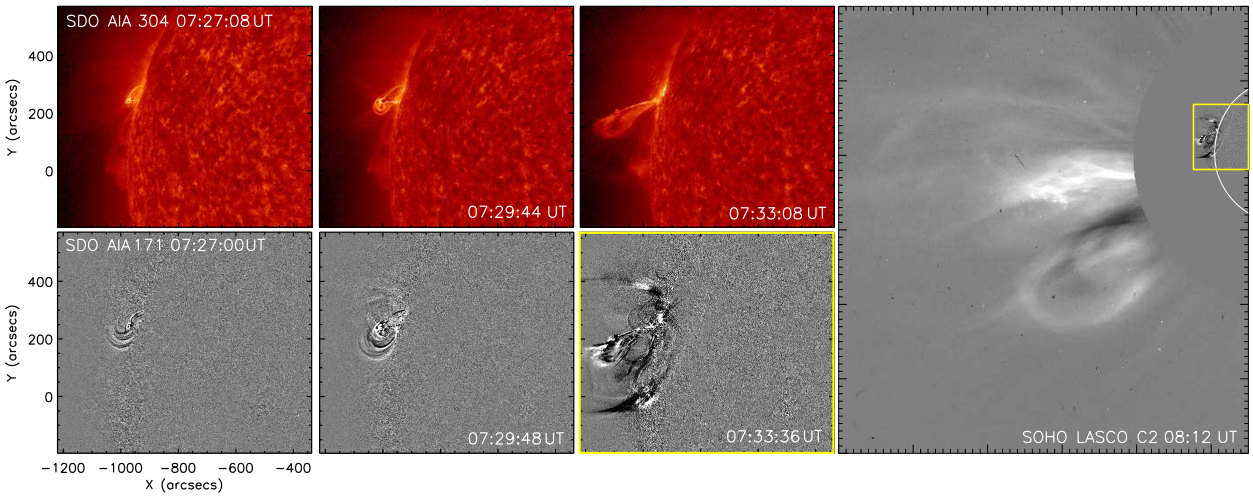

Fig. 1.— Left: Observations of SDO/AIA of the erupting filament. The 304 Å channel shows direct images (movie in online version), the 171 Å channel the corresponding running difference images. Right: Observations of SOHO/LASCO of the associated CME. The yellow rectangle shows the AIA 171 Å running difference image about 30 minutes prior to the LASCO observations.

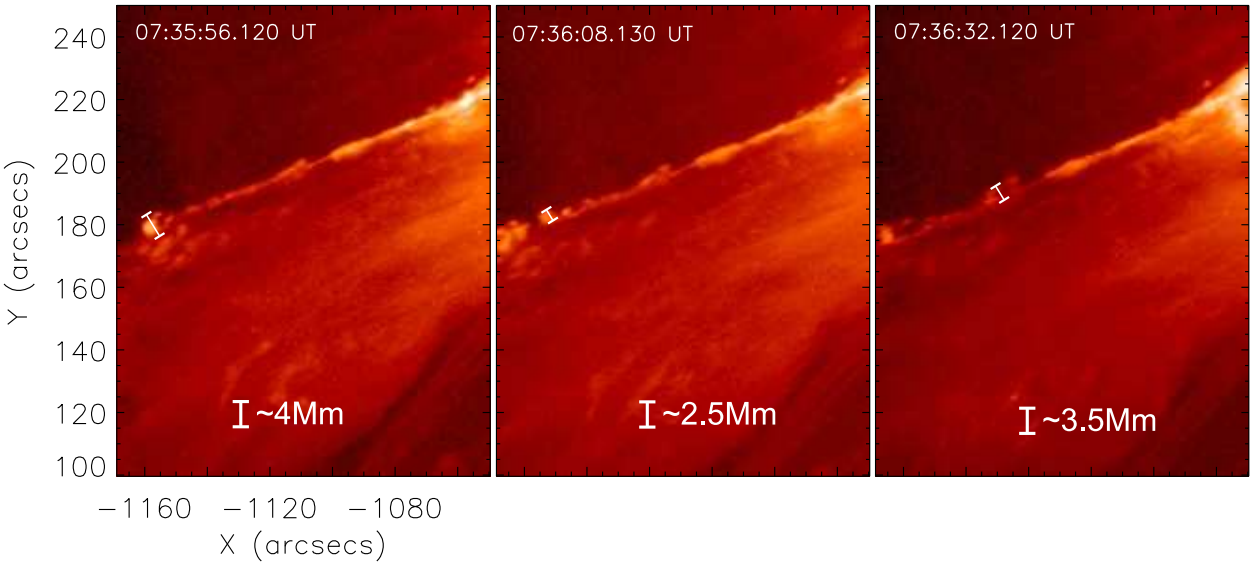

Fig. 2.— Zoom into the AIA 304 Å images, showing the northern boundary of the filament and indicating the height of the observed structures.

The vortex structures are best observed in the AIA 304 Å passband ($T \approx 0.5$ MK, see Figures 1 and 2). Wavebands imaging the outer corona in temperatures between 0.4 MK - 2 MK (131 Å, 171 Å, 193 Å and 211 Å) show only the parts of the vortices close to the boundary layer.

Measuring the front of the filament, we derive an average speed of ≈ 470 km s^{-1}. The height of the structures lies in the range of 2.5 to 4 Mm (Figure 2). In Figure 3 we show cuts along the northern edge of the filament for different times. These plots clearly reveal the quasi-periodic appearence of the vortex-like structures, their evolution and propagation with time, which allows us to estimate characteristic quantities from these observations. The spatial period of the vortex-like structures is found to be approximately $20''$ (Figure 3), which corresponds to a wavelength λ of approximately 14.4 Mm. The average propagation speed $v_{\rm prop}$ of the observed structures along the boundary is about 310 ± 20 km s^{-1}. Since this event occurred on the limb of the Sun, we can neglect projection effects.

3. Simulation Setup

We solve the ideal MHD equations numerically with the so-called TVD Lax-Friedrichs scheme (Tóth & Odstrčil 1996). The numerical algorithm was already used in previous studies on the Kelvin-Helmholtz instability (Amerstorfer et al. 2010; Möstl et al. 2011; Zellinger et al. 2012).

We estimate the plasma parameters in the corona using typical values, which can be found in the literature (Aschwanden 2004). In the corona, the electron density n_e is taken to be 1×10^{15} m^{-3}, the plasma pressure p is 0.09 Pa, and the magnetic field B is 10×10^{-4} T. With these values, we obtain for the total pressure $\Pi = 0.5$ Pa, which is the sum of plasma and magnetic pressures. In the filament, we assume that the density is at least 10

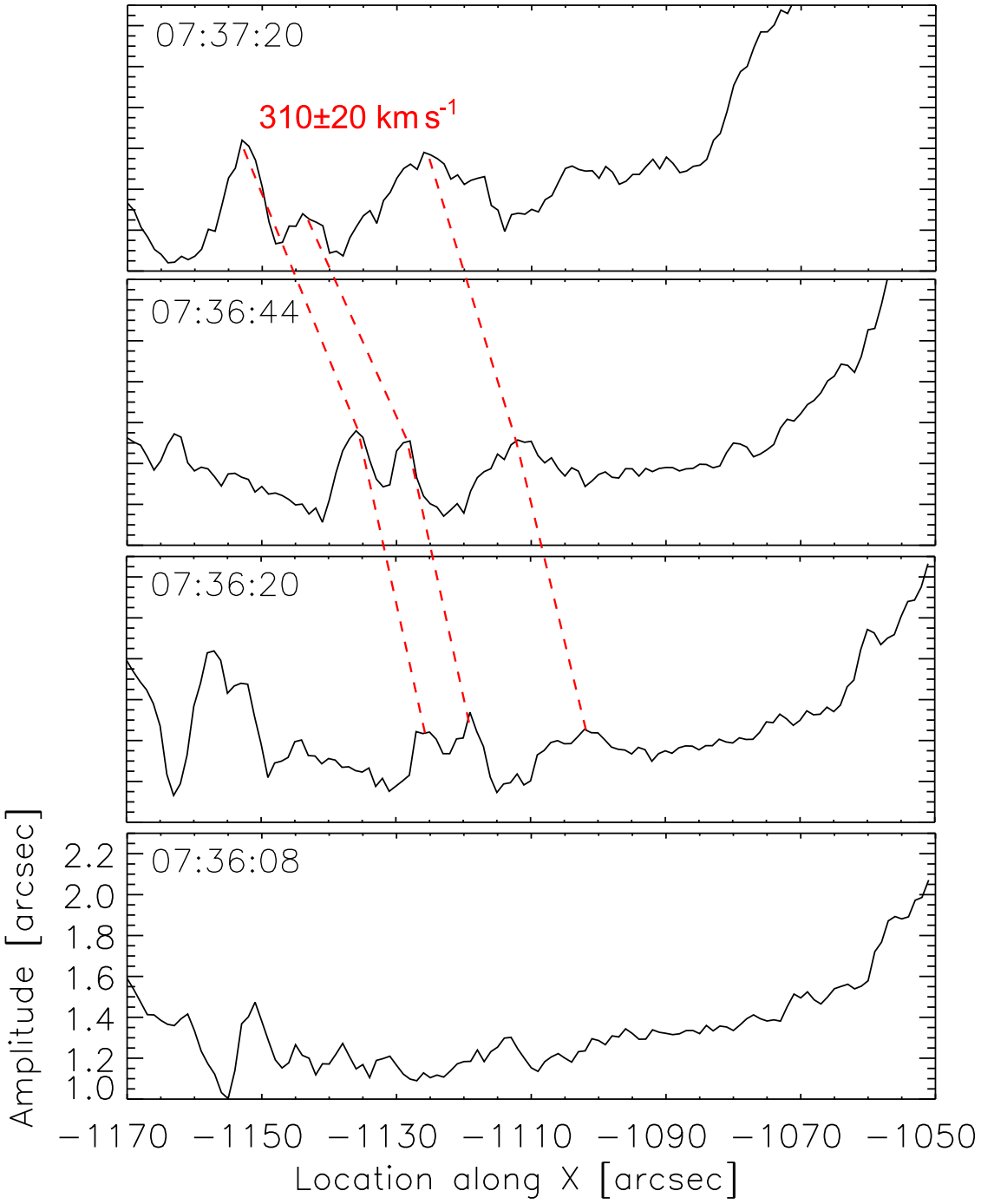

Fig. 3.— Profiles of the quasi-periodic structures along the northern boundary layer of the filament for different times, measured from direct images in the AIA 304 $\AA$ channel. The time is given in UT. The propagation speed of these structures is about 310 ± 20 km s^{-1}.

times higher than the corona value and that $T \leq 1 \times 10^5$ K. With further assumptions that $n_i \approx n_e = n$ and $T_i \approx T_e = T$ we have for the plasma pressure $p = 2\,n\,k\,T = 0.028$ Pa. The subscript i denotes the values for the ions. We take 450 km s^{-1} as the approximate speed of the filament v_f and assume that the surrounding coronal plasma moves at half of this speed. These plasma parameters are used as input for the simulations.

The general setup for the simulations is such that the x-direction is along the boundary layer and the y-direction is perpendicular to it. This means that the plasma parameters change in y-direction, and the disturbances (vortices) propagate along the x-direction. The background plasma parameters vary according to a tanh-profile. Thus, we do not have a tangential discontinuity, but the boundary layer has some finite thickness.

As initial condition we need an equilibrium plasma configuration. In ideal MHD simulations, this means that the total pressure Π has to be constant across the boundary layer, i.e. in our case

$$\frac{\partial \Pi}{\partial y} = 0\,, \tag{1}$$

with

$$\Pi = p + \frac{B^2}{2\,\mu_0}\,, \tag{2}$$

where p is the thermal pressure, B is the magnetic field and μ_0 is the permeability in vacuum. In order to have an initial equilibrium, we determine the total and the plasma pressure from the plasma background parameters and then calculate the magnetic field according to

$$B = \sqrt{2\,\mu_0\,(\Pi - p)}\,. \tag{3}$$

For the cases, where we have two magnetic field components, B_x and B_z, we assume a constant B_x and then use Equation 3 to calculate B_z. Onto this equilibrium we impose small random initial disturbances of v_x and v_y, with an amplitude of 1% of the initial filament velocity.

We use normalized quantities in the numerical simulations. The normalization constants are the initial filament speed v_f, the filament mass density ρ_f and the half-width of the boundary layer a. Accordingly, the time is then normalized with a/v_f, the pressures with $\rho_f\, v_f^2$ and the magnetic field with $\sqrt{\mu_0\, \rho_f\, v_f^2}$. The computational box extends from 0 to $50\, a$ in x-direction and from $-25\, a$ to $25\, a$ in y-direction. At the x-boundaries we impose periodic boundary conditions and at the y-boundaries transmissive ones.

4. Results

The top panel of Figure 4 shows the (normalized) mass density for different (normalized) times in the simulation run. The blue layer represents the surrounding coronal plasma, whereas the red layer is the ejected filament. For this simulation run, only a z-component of the magnetic field was taken on both boundaries. The x- and y-components of B are zero, as well as the z-component of the velocity. The plasma flows from right to left. After some time, small initial perturbations grow in amplitude and eventually reach their nonlinear vortex phase. Then, a saturation sets in and the regular vortex-structures become irregular, as does the whole boundary layer. At $t \approx 200$ the vortices have fully formed on both boundary layers. However, the observations show vortices only on one side of the filament boundary.

From theory it is known that a magnetic field parallel to the boundary layer can have a stabilizing effect on the KHI due to magnetic field line tension. The Alfvén Mach number M_A, determined only with the parallel magnetic field component, has to be larger than 2 for the instability to develop. Combining the effects of compressibility and magnetic field line tension results in the instability condition that $2\, v_A < \Delta v \leq 2\, v_s$, where Δv is the total velocity jump across the boundary layer, v_A is the Alfvén velocity and v_s the sound

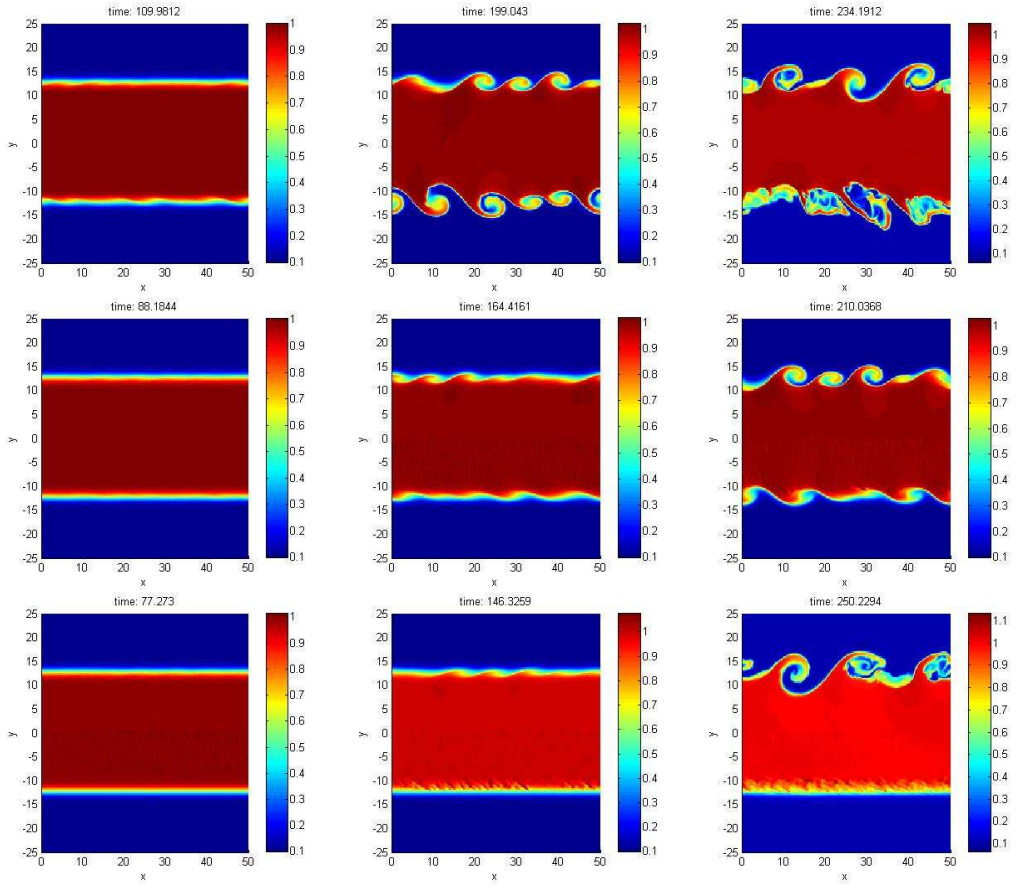

Fig. 4.— Time series of the mass density (color code). The plasma flows from right to left. Top panel: Only a z-component of the magnetic field was assumed. Middle panel: An x-component of the magnetic field of 10% of the total magnetic field strength was assumed. Bottom panel: An x-component of the magnetic field of 20% of the total magnetic field strength was assumed (movies in online version).

velocity, or equivalently $v_A < v_s$ (for the exact derivation of the instability criterion we refer to Miura and Pritchett 1982). We performed simulations including an x-component of the magnetic field at the lower boundary layer to derive the field strength needed to stabilize the boundary layer.

The middle and bottom panels of Figure 4 show the results of two simulation runs where an x-component of the magnetic field is included at the lower boundary layer. The middle panel is the result with $B_x = 0.1\,B$ and the bottom panel with $B_x = 0.2\,B$. For the first case, there are still vortices visible at the lower boundary, whereas for the latter case, the parallel magnetic field is large enough to stabilize the boundary layer. This stabilizing effect of a strong parallel B (Chandrasekhar 1961) is a possible reason why the vortices are only observed on one side of the erupting filament.

From the simulation that most closely resembles the observations (bottom panel of Figure 4), we determine the wavelength λ (i.e. the distance between two vortices) and the height h of the vortex-structure. We derive an approximate λ of about 10 to $15\,a$ and an approximate h of about 3 to $5\,a$.

In order to get physical values, we have to make an estimation of the half width of the shear layer a. From the observations shown in Figure 2, we can estimate the boundary layer to be about 1 to 2 Mm, resulting in $a \approx 0.5 - 1$ Mm. Taking these values, the wavelength and the height of the simulated structures yield (i) $\lambda \approx 5 - 7.5$ Mm and $h \approx 1.5 - 2.5$ Mm, or (ii) $\lambda \approx 10 - 15$ Mm and $h \approx 3 - 5$ Mm, respectively. The propagation velocity $v_{\rm prop}$ of the simulated KH vortices lies around 330 km s^{-1}. All of these characteristic features of the simulated instability are in basic quantitative agreement with the observations ($\lambda \approx 14.4$ Mm, $h \approx 2.5 - 4$ Mm, $v_{\rm prop} \approx 310 \pm 20$ km s^{-1}). Furthermore, we find that a B_x of approximately 2×10^{-4} T is needed to stabilize the lower boundary layer.

Qualitatively, we can compare the structure of the simulated vortices with the

observations. Figure 5 shows on the left side the evolution of the simulated KH vortices and on the right side the profiles through the vortices for each time step. A rather characteristic double peak appears when the vortices are rolled-up. Such double peaks are also visible in the profiles obtained from the direct images presented in Figure 3. Another feature associated with an instability is a growing amplitude of the perturbations, which is seen in both, simulations and observations (Figures 5 and 3, respectively).

5. Discussion and Conclusions

There are various important implications resulting from the occurrence of the KHI at the boundaries of CMEs. As Foullon et al. (2011) discuss, the KHI at CME surfaces may affect the drag force (Vršnak et al. 2012), and hence, the CME kinematics in interplanetary space and its geoeffectiveness. Due to reconnection inside KH vortices, a plasma transport across the boundary can be initiated (e.g. Nykyri and Otto 2004) leading to a mass loss of the CME. Additionally, magnetic reconnection can lead to the erosion of the initial magnetic flux, again influencing the geoeffectiveness of CMEs (Dasso et al. 2007; Taubenschuss et al. 2010; Ruffenach et al. 2012).

We present numerical simulations of the KHI on a boundary of a filament embedded in a CME. We find qualitative as well as quantitative agreements between the simulation results and the observed features of quasi-periodic vortex-like structures observed at the northern boundary of a filament during an eruption on 2011 February 24. Additionally, we have shown that a magnetic field component parallel to the boundary layer with a strength of about $0.2\,B$, corresponding in our case to 2×10^{-4} T, results in a stabilization of the boundary layer and could be an explanation of the observed asymmetric development of the vortex-like structures. Our assumption of a tenfold density jump towards the filament is a

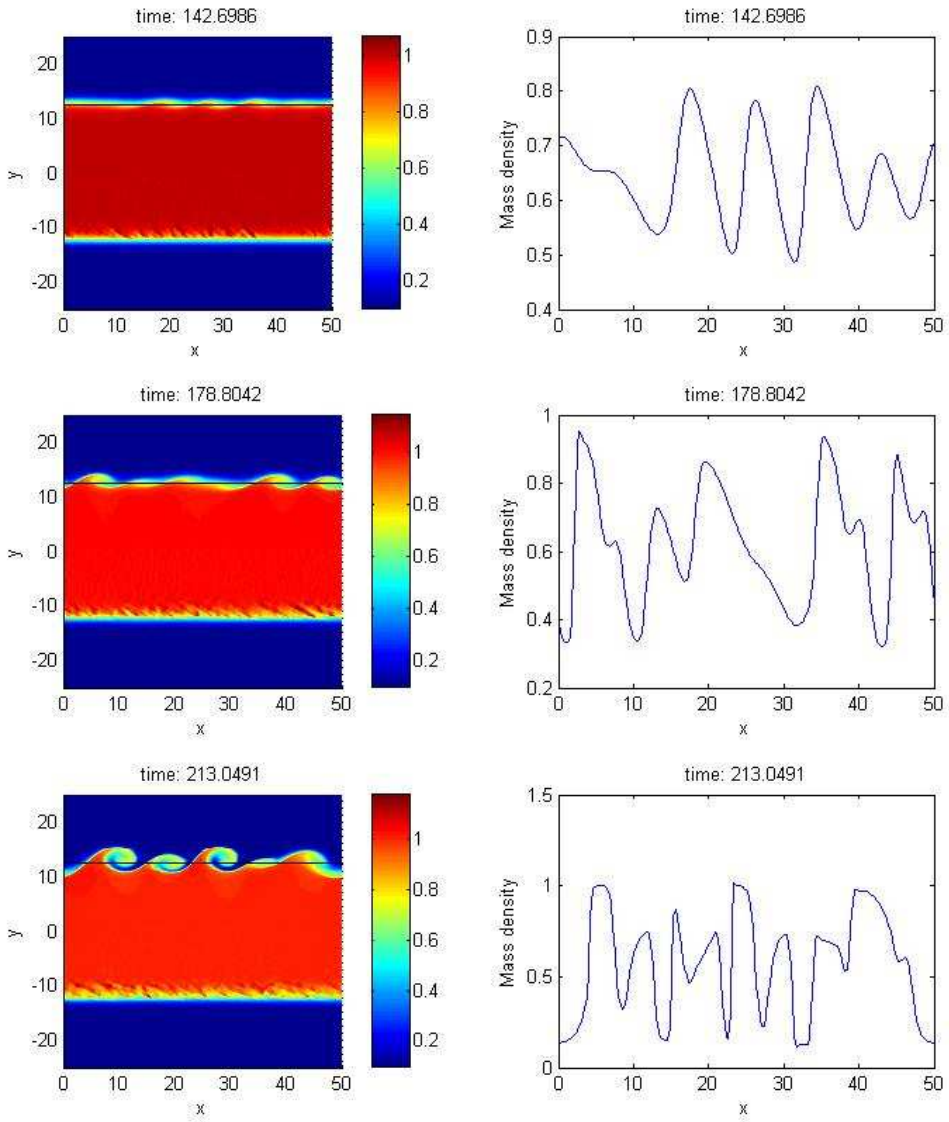

Fig. 5.— Left: Evolution of the KH vortices. The black lines indicate, where the cuts shown on the right plots were taken. Right: Profiles of the density through the vortices at different time steps.

very conservative one, as one can expect a larger density increase of about 100 or more. As was shown in previous studies (Amerstorfer et al. 2010; Möstl et al. 2011), a larger density ratio results in smaller instability growth rates and, thus, it exhibits a stabilization of the boundary layer. Contrary to this stabilizing effect, a larger velocity shear than the one assumed in this case study would act destabilizing.

The numerical MHD model applied is of course an idealized one with simplifying assumptions of the geometry of the CME and of the parameters. The model uses standard input plasma parameters, which are typical for the observed features but may differ for this specific event. Nevertheless, it captures important basic physical properties of the studied boundary layer processes. We point out that we are limited in observations coming from a single vantage point. The vortex structures might be affected by projection effects and possibly signatures of twisted field lines (flux rope), viewed from aside, may show similar structures.

The stabilizing effects might be large enough, such that the KHI is only seldomly able to develop at CME boundaries in the solar corona. For the present case study we found evidence for the occurrence of the KHI on boundary layers in the solar corona. More observational data of possible KHI formation are needed to better understand its physics and its consequences on propagating MHD structures.

UVM, MT and AMV gratefully acknowledge the Austrian Science Fund (FWF): P21051-N16, V195-N16 and P24092-N16.

Facilities: SDO (AIA)

REFERENCES

Amerstorfer, U. V., Erkaev, N. V., Taubenschuss, U., & Biernat, H. K. 2010, Phys. Plasmas, 17, 072901

Andries, J., & Goossens, M. 2001, A&A, 368, 1083

Aschwanden, M. J. 2004, Physics of the Solar Corona. An Introduction (Chichester: Praxis Publishing Ltd)

Battaglia, M., & Kontar, E. P. 2011, A&A, 533, L2

Chandrasekhar, 1961, Hydrodynamic and hydromagnetic stability (Oxford: Clarendon Press)

Dasso, S., Nakwacki, M. S., Démoulin, P., & Mandrini, C. H. 2007, Sol. Phys., 244, 115

Foullon, C., Verwichte, E., Nakariakov, V. M., Nykyri, K., & Farrugia, C. J. 2011, ApJ, 729, L8

Heyvaerts, J., & Priest, E. R. 1983, A&A, 117, 220

Innes, D. E., Cameron, R. H., Fletcher, L., Inhester, B., & Solanki, S. K. 2012, A&A, 540, L10

Karpen, J. T., Antiochos, S. K., Dahlburg, R. B., & Spicer, D. S. 1993, ApJ, 403, 769

Kolesnikov, F., Bünte, M., Schmitt, D., & Schüssler, M. 2004, A&A, 420, 737

Lemen, J. R., Title, A. M., Akin, D. J., et al. 2012, Sol. Phys., 275, 17

Martínez Oliveros, J.-C., Hudson, H. S., Hurford, G. J., et al. 2012, ApJ, 753, L26

Miura, A. 1997, Phys. Plasmas, 4, 2871

Miura, A., & Pritchett, P. L. 1982, J. Geophys. Res., 87, 7431

Möstl, U. V., Erkaev, N. V., Zellinger, M., et al. 2011, Icarus, 216, 476-484

Nykyri, K., & Otto, A. (2004), Ann. Geophys., 22, 935

Ofman, L., & Thompson, B. J. 2011, ApJ, 734, L11

Pesnell, W. D., Thompson, B. J., & Chamberlin, P. C. 2012, Sol. Phys., 275, 3

Rae, I. C. 1983, A&A, 126, 209

Ruffenach, A., Lavraud, B., Owens, M. J., et al. 2012, J. Geophys. Res., 117, A09101

Ryutova, M., Berger, T., Frank, Z., Tarbell, T., & Title, A. 2010. Sol. Phys., 267, 75

Soler, R., Terradas, J., Oliver, R., Ballester, J. L., & Goossens, M. 2010, ApJ, 712, 875

Soler, R., Díaz, A. J., Ballester, J. L., & Goossens, M. 2012, ApJ, 749, 163

Taroyan, Y. 2011, A&A, 533, A68

Taubenschuss, U., Erkaev, N. V., Biernat, H. K., et al. 2010, Ann. Geophys., 28, 1075

Tóth, G., & Odstrčil, D. 1996, J. Comp. Phys., 128, 82

Vršnak, B., Žik, T., Vrbanec, D., et al. 2012, Sol. Phys., doi:10.1007/s11207-012-0035-4

Zaqarashvili, T. V., Díaz, A. J., Oliver, R., & Ballester, J. L. 2010, A&A, 516, A84

Zellinger, M., Möstl, U. V., Erkaev, N. V., & Biernat, H. K. 2012, Phys. Plasmas, 19, 022104

This manuscript was prepared with the AAS LaTeX macros v5.2.